Available online at www.sciencedirect.com
ScienceDirect
Journal of Organometallic Chemistry 693 (2008) 77–86
Journal of Organometallic Chemistry
www.elsevier.com/locate/jorganchem

Cobalt(II) complexes with disubstituted 3-aminopyrazole derivative: Mononuclear Co(II) complex with in situ prepared formamidine ligand ☆

Vukadin M. Leovac [a], Zoran D. Tomić [b], Attila Kovács [c], Milan D. Joksović [d], Ljiljana S. Jovanović [a], Katalin Mészáros Szécsényi [a,*]

[a] *Faculty of Sciences, University of Novi Sad, Trg D. Obradovića 3, 21000 Novi Sad, Serbia*
[b] *"Vinča" Institute of Nuclear Sciences, Laboratory of Theoretical Physics and Condensed Matter Physics, P.O. Box 522, 11001 Belgrade, Serbia*
[c] *Research Group for Materials Structure and Modeling of the Hungarian Academy of Sciences, Budapest University of Technology and Economics, H-1111 Budapest, Szt. Gellért tér 4, Hungary*
[d] *Faculty of Sciences, University of Kragujevac, R. Domanovića 12, 34000 Kragujevac, Serbia*

Received 6 August 2007; received in revised form 8 October 2007; accepted 11 October 2007
Available online 18 October 2007

Abstract

In the reaction of $Co(NO_3)_2 \cdot 6H_2O$ with 4-acetyl-3-amino-5-methylpyrazole (*aamp*) two octahedral Co(II) complexes, $[Co(aamp)_2(H_2O)_4](NO_3)_2$, **1**, and $[Co(ampf)(MeOH)_2NO_3]NO_3$ (*ampf* = N,N′-bis(4-acetyl-5-methylpyrazole-3-yl)formamidine), **2**, were obtained, depending on the reaction conditions. The presence of water in the reaction system leads to incorporation of water molecules into the crystal lattice and **1** was formed. In an anhydrous environment, due to addition of $CH(OEt)_3$, the fusion of two *aamp* was induced through their NH_2-groups, incorporating the methine group of $CH(OEt)_3$. As a result, complex **2**, containing an adenino-mimetic NNO pharmacophore ligand, was obtained. The crystal and molecular structure of both compounds was determined. The coordination of *aamp* in **1** was achieved through N2 of the pyrazole ring. On the contrary, in **2**, an unusual coordination mode of pyrazole is found: one of the pyrazole moieties, due to steric hindrance, coordinates through the oxygen atom of the acetyl group instead of N2. The complexes were characterized by elemental analysis and electronic spectra. For **2** a comprehensive IR spectral analysis is given. The metal–ligand interactions in **2** are analyzed by quantum chemical computations. The desolvation mechanism of both compounds is discussed in detail.

Keywords: Cobalt(II); 4-Acetyl-3-amino-5-methylpyrazole; Formamidine; FT-IR; DFT computations

1. Introduction

Our interest in pyrazole-based ligands and their transition metal complexes has lasted about two decades because of their attractive physicochemical, chemical, structural and biological properties [1–3]. Among them 3-aminopyrazole and its derivatives serve as useful entry into pyrazole chemistry. The heterocyclic naphthoquinones, synthesized from 3-aminopyrazole, exhibit significant antiprotozoal and cytotoxic activity [4]. Pyrazolo[1,5-a]pyrimidines, as purine analogues derived from corresponding 3-aminopyrazole derivatives have attracted wide pharmaceutical interest because of their estrogen receptor β antagonist activity [5], HMG-CoA reductase inhibitor activity [6] and AMP phosphodiesterase inhibitor activity [7]. However, the chemistry of 3-aminopyrazole has remained largely underdeveloped until the discovery of its derivatives as antitumor agents with their inhibitory activity of cyclin-dependent kinases (CDKs), a family of enzymes that

☆ Transition metal complexes with pyrazole based ligands. Part 26 (This paper).

* Corresponding author. Tel.: +381 21 485 2741; fax: +381 21 454 065.
E-mail address: mszk@uns.ns.ac.yu (K.M. Szécsényi).

0022-328X/$ - see front matter © 2007 Elsevier B.V. All rights reserved.
doi:10.1016/j.jorganchem.2007.10.018

are regulated by phosphorylation and activated by their association with cyclins [8–10].

In accordance with the newest trends in coordination chemistry, the aim of our studies is to get a better insight into the most relevant factors determining the course of complex formation, including the position and type of donor atoms, the steric repulsion and effect of solvent [11–13]. As a part of our present interest towards such pyrazole ligands, we have designed a new compound based on the 3-aminopyrazole moiety, an important adenino-mimetic pharmacophore present in several classes of kinase inhibitors. The –NH–CH=N– pattern of 3-aminopyrazole, which is stereochemically well suited to form hydrogen bonding interactions with the kinase hinge region, was embedded in the novel *N*,*N*′-bis(4-acetyl-5-methylpyrazole-3-yl)formamidine (*ampf*) ligand obtained in situ by a one-step template synthesis. Due to its numerous donor groups, *ampf* has diverse possibilities of coordination.

To see how the experimental conditions affect the course of formation of complexes with 4-acetyl-3-amino-5-methylpyrazole (*aamp*) we have prepared complexes of Cu(II) [1], Co(II) [14,15], Zn(II) [1,16], Hg(II) [1] and Pt(II) [2] with the *aamp* ligand. It was found that in its neutral form this ligand coordinates mostly monodentately through the N2 nitrogen atom of the pyrazole ring. The complex of $[PtCl(\mu\text{-}aamp\text{-}H)(Me_2SO)]_2$ is obtained by thermal conversion of *trans*-$[PtCl_2(aamp)(Me_2SO)]$, which means a bidentate coordination mode of *aamp* through an N^1N^2 bridge [2]. N^1N^2-bridge formation was also observed in $[Zn(\mu\text{-}aamp\text{-}H)(aamp)OAc]$ [16]. In our earlier papers [14] the syntheses, some physicochemical properties and thermal characterization [15] of tetrahedral $[Co(aamp)_2X_2]$ (X = Cl, Br, I, NCS, NCO), the pseudo-octahedral $[Co(aamp)_2(H_2O)_4](NO_3)_2$ and that of $[Co\{\mu\text{-}N(CN)\}_2(aamp)_2]$ has been reported. All these reactions were carried out in the presence of a small amount of water originating from the crystal hydrates of the metal salts used in the synthesis. Taking into account the coordination requirement of central atom and the intention to see how the absence of water influences the complex formation of *aamp* with $Co(NO_3)_2$, we carried out the reaction in the presence of the dehydrating agent $CH(OEt)_3$, in a methanolic solution, having in mind that $CH(OEt)_3$ with amines like *aamp* may take part in a formamidine bridge formation [17]. In this way we tried to secure the reaction conditions to formation of a compound with a tailored structure, containing –NH–CH=N– group. Copper(II) complexes with formamidine ligands have been prepared by template synthesis from 2-aminopyridine derivatives [17]. Attempts of the same authors to apply this method to prepare compounds with metals other than Cu(II) have failed. Our present work describes the novel $[Co(ampf)(MeOH)_2NO_3]NO_3$ complex with a formamidine ligand, formed in an easy, one-step synthesis using 3-aminopyrazole precursor and orthoester as a dehydrating and ligand forming agent. This complex is characterized by elemental analysis, X-ray diffraction, FT-IR and UV–Vis spectroscopy and thermal analysis while the metal–ligand interactions were studied by quantum chemical calculations. We report here also the X-ray diffraction and UV–Vis spectral data of the previously synthesized $[Co(aamp)_2(H_2O)_4](NO_3)_2$ complex [14]. In the view of the corresponding crystal structures of both complexes their desolvation is discussed.

2. Experimental and computational details

2.1. Synthesis of the complexes

All chemicals used were commercial products of analytical reagent grade.

The preparation and some physicochemical characteristics of $[Co(aamp)_2(H_2O)_4](NO_3)_2$ are described in our previous paper [14]. Here only additional data are presented. Elemental analysis data, $C_{12}H_{26}CoN_8O_{12}$ ($M_r = 533.32$): C, 27.03; H, 4.91; N 21.01. Found: C, 27.52; H, 4.84; N, 21.04%. UV–Vis (MeOH), λ_{max}/nm (ε/dm^3 mol^{-1} cm^{-1}): 237 (10500), 282 (6300), 467 (3), 513 (4), 1041 (2). Its crystal and molecular structure is discussed, too.

For the synthesis of $[Co(ampf)(MeOH)_2NO_3]NO_3$, $Co(NO_3)_2 \cdot 6H_2O$ (0.32 g, 1.1 mmol) was dissolved in warm MeOH (10 cm^3) and mixed with solid *aamp* (0.20 g, 1.4 mmol). To the solution $CH(OEt)_3$ was added (4 cm^3) and the mixture was mildly heated for 2–3 min. The solvent was evaporated at room temperature for 2 days until rose crystals were precipitated. The crystals were separated, washed with MeOH and air dried. Yield: 0.16 g (37% calculated on the basis of *aamp*). Elemental analysis data, $C_{15}H_{24}CoN_8O_{10}$ ($M_r = 535.33$): C, 33.65; H, 4.59; N, 20.94%. Found: C, 33.71; H, 4.39; N, 20.72%. UV–Vis (MeOH), λ_{max}/nm (ε/dm^3 mol^{-1} cm^{-1}): 250 (2300), 312 (6900), 479 (19), 494 (6), 661sh (2), 1035 (3). Molar conductivity, λ_M(MeOH) = 164 Scm^{2}mol^{-1}. $\mu_{eff} = 5.00\ \mu_B$.

2.2. Elemental analysis

Elemental (C, H, N) analyses were performed by standard micromethod.

2.3. Spectral data collection

FT-IR spectra of solid **2** were recorded on a Perkin–Elmer System 2000 FT-IR spectrometer equipped with an MCT (mercury cadmium telluride) detector for the mid-IR range and with a DTGS (deuterated triglycine sulfate) detector for the far-IR (450–50 cm^{-1}) range. The mid-IR spectra were measured using KBr pellets and 16 scans while in the far-IR experiments polyethylene pellets and 128 scans were applied. In all the measurements the resolution was 4 cm^{-1}.

Electronic spectra of 2×10^{-3} mol/dm^3 MeOH solutions of the complexes were recorded on a Secomam (Anthelie 2, Advanced, for the spectral range of 220–900 nm) spectro-

photometer and on a Thermo Nicolet instrument (NEXUS 670 FT-IR, for the range 900–1400 nm).

2.4. Thermal analysis

Thermal analysis was performed using a DuPont 1090 TA system with sample masses of about 5 mg. The thermogravimetric measurements were carried out in a platinum crucible. DSC curves were recorded up to 600 K using an open aluminum pan sample holder with an empty aluminum pan as reference. The measurements were conducted in argon with a gas flow rate of 1.5 dm^3/min and a heating rate of 10 K/min.

2.5. Magnetic and molar conductivity measurements

The magnetic susceptibility of **2** was measured at room temperature using an MSB-MKI magnetic susceptibility balance, Sherwood Scientific Ltd., Cambridge. Molar conductivity data of freshly prepared 1×10^{-3} mol/dm^3 solution in MeOH was obtained at room temperature by a digital conductivity meter Jenway 4010.

2.6. Crystal structure determination and refinement

Both single crystal X-ray diffraction experiments were carried out on Bruker AXS SMART three-circle diffractometer equipped with CCD detector, using 0.3 degree omega scans and Mo Kα radiation at a temperature of 120 K. The crystal structures of **1** and **2** were solved by direct methods using the SIR92 software [18] and refined by the Oxford Crystals suite [19]. The nonhydrogen atoms in both structures were refined anisotropically. The hydrogen atoms in compound **1** were located from difference Fourier maps and refined isotropically, hydrogen atoms in the crystal structure of **2** were refined isotropically using restraints. Molecular graphics were created using the programs Ortep [20] and Mercury [21].

2.7. Quantum chemical computations

The geometry optimization and computation of the harmonic vibrational frequencies of **2** were carried out using the Becke3–Lee–Yang–Parr (B3LYP) exchange-correlation functional [22,23] in conjunction with a 6-31G** basis set. For Co a relativistic effective core potential [24] was used extended by a single set of *f*-type polarization functions [25]. The geometry optimization was started from the Cartesian coordinates obtained in the X-ray diffraction analysis. The complex possesses an open-shell electronic structure with three unpaired electrons (multiplicity = 4). All the quantum chemical computations were performed with the GAUSSIAN03 program [26]. The natural bond orbital (NBO) analysis [27] has been performed with the NBO3.0 code [28] implemented in GAUSSIAN03.

3. Results and discussion

3.1. Synthesis of the complexes

The ligand (4-acetyl-3-amino-5-methylpyrazole, *aamp*) gives with $Co(NO_3)_2 \cdot 6H_2O$ in EtOH a pseudo-octahedral complex **1** where the coordination sphere of the central ion is occupied by four water molecules (see Scheme 1) as the nitrate ion is usually a poor ligand in the presence of water. With cobalt(II) halides and pseudo-halides under identical reaction conditions tetrahedral [Co(*aamp*)$_2$X$_2$] complexes are formed [14], *i.e.*, neither H_2O nor EtOH is involved in the coordination. As halides coordinate readily and the coordination ability of EtOH is low, the structure of these complexes is in accordance with the expectations.

With an idea of producing an adenino-mimetic pharmacophore, we accepted a challenging task to explore what would happen in an anhydrous solution, in the presence of $CH(OEt)_3$ excess which is a known dehydrating and in the same time a CH-group supplying agent [29] for insertion purposes. Under this reaction condition the formation

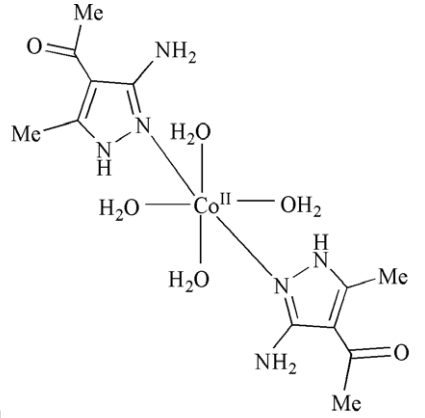

1

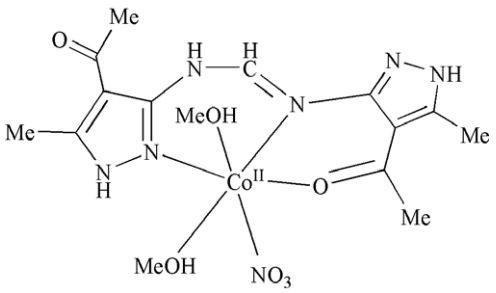

2

Scheme 1.

of a formamidine group becomes very probable. We have used MeOH as a solvent whose coordination ability lies between H_2O and EtOH. In this way we could also trace the effect of the solvent to the complex formation process. As a result, we obtained complex **2** with a novel tridentate NNO ligand (see Scheme 1) consisting of two 4-acetyl-5-methylpyrazole moieties connected through a formamidine bridge in which the CH group comes from $CH(OEt)_3$. Such behavior of $CH(OEt)_3$ with amines has already been observed [17]. The most probable reaction mechanism of the –NH–CH=N– bridge formation is depicted in Scheme 2. Yet, our efforts to obtain the ligand itself according to literature procedures, without the presence of Co(II), have failed.

On the other hand, it should be mentioned that the role of an orthoester in complex formation reactions may be diverse, depending on the ligand. The reaction of 3,5-dimethyl-1-(hydroxymethyl)-pyrazole with $Cu(NO_3)_2 \cdot 6H_2O$ in the solvent mixture methanol-propan-2-ol, in the presence of trimethyl orthoformate results in a dimeric, five coordinated complex of Cu(II) with 3,5-dimethylpyrazole, 3,5-dimethyl-1-(methoxy)-pyrazole and nitrato ligands [30]. By in situ decomposition of triethyl orthoformate, 4-aminopyridine (4*ap*) with Cu(II) gives a polymeric *catena*-$[Cu(4ap)_2(HCO_2)_2]$ [31].

3.2. Crystal and molecular structures of the complexes

The crystallographic details for **1** and **2** are given in Table 1.

The crystal structure of **1** is built up of centrosymmetric $[Co(aamp)_2(H_2O)_4]^{2+}$ cations (Fig. 1) and NO_3^- anions. The central Co(II) ion is located on the crystallographic inversion center in a configuration being nearly octahedral. The coordination polyhedron is defined by the two N2 of the pyrazole rings (in Fig. 1 marked as N13) in *trans* position and two water molecules in the equatorial plane, while

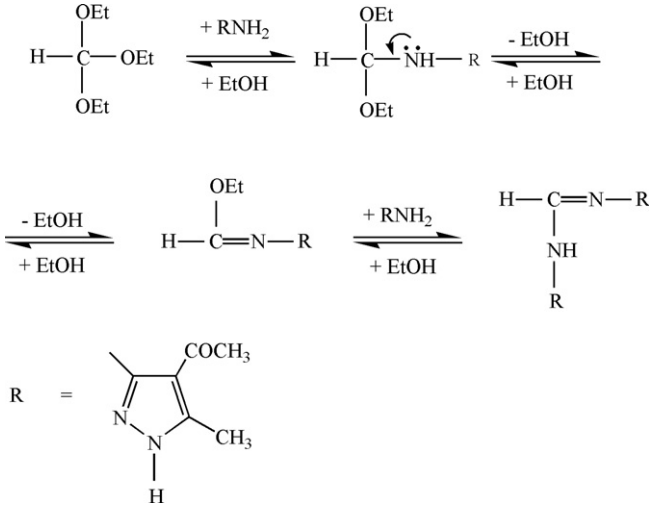

Scheme 2. Possible pathway for the formation of formamidine from orthoester.

Table 1
Crystallographic data for **1** and **2**

Compound	**1**	**2**
Formula	$C_{12}H_{26}CoN_8O_{12}$	$C_{15}H_{24}CoN_8O_{10}$
Formula weight	533.32	535.33
Crystal system	Monoclinic	Triclinic
Space group	$C2/c$	$P\bar{1}$
a (Å)	18.4009(8)	7.6049(7)
b (Å)	6.7027(3)	10.5979(9)
c (Å)	17.1569(7)	14.7350(13)
α (°)		95.830(2)
β (°)	93.965(1)	102.217(2)
γ (°)		105.998(2)
V (Å^3)	2110.99(16)	1099.46(17)
Z	4	4
D_{calc} (gm/cm^3)	1.678	1.617
M (Mo Kα)	0.893	0.851
Temperature (K)	293	293
λ (Mo Kα)	0.71073	0.71073
2θ Range	2.2–30.0	1.4–30.0
Reflections collected	14213	12717
Unique reflections	3085	5866
Reflections observed, $[I > 2\sigma I]$	2973	3657
R_{int}	0.015	0.021
Number of parameters	203	307
R $[I > 2\sigma I]$	0.0428	0.0384
wR_2 $[I > 2\sigma I]$	0.0930	0.0998
Goodness-of-fit on F^2	0.96	0.92
Residual density (e/Å^3)	−0.41/1.16	−0.66/0.54

the other two water molecules are coordinated at axial positions. The pyrazole ligand is coordinated in a monodentate fashion, at a Co–N distance of 2.159(1) Å. Selected bond lengths and angles are given in Table 2 while the nonbonding interactions, relevant for the association of the molecules are presented in Table 3.

A comparison of the coordinated ligand geometry with that of the free 4-acetyl-3-amino-5-methylpyrazole [1] did not reveal significant influence of the coordination on the ligand geometry. However, some differences in the geometry of the free and coordinated ligand indicate possible influence of the nonbonding contacts on the ligand geometry. Thus, the C–N(amino) bond of 1.342(2) Å is slightly shorter than the equivalent bonds of the uncoordinated ligand (1.364(5) and 1.368(4) Å [1]). This may be attributed to the involvement of this amino group in the hydrogen bonds in the crystal structure of uncoordinated ligand. In the complex, the amino group does not participate in any hydrogen bonds.

Association of the complex molecules in the solid state is determined by the presence of coordinated water molecules as hydrogen bond donors at the axial positions and oxygen atoms from the carbonyl groups in the equatorially coordinated ligand, which serve as hydrogen bond acceptors. With participation of a nitrate in the stabilization of the crystal structure these contacts lead to the formation of the 3D arrangement, shown in Fig. 2. Hydrogen atoms bonded to the pyrazole ring and the amino-N are not involved in intermolecular contacts, relevant for the association of the molecules. When a possible influence

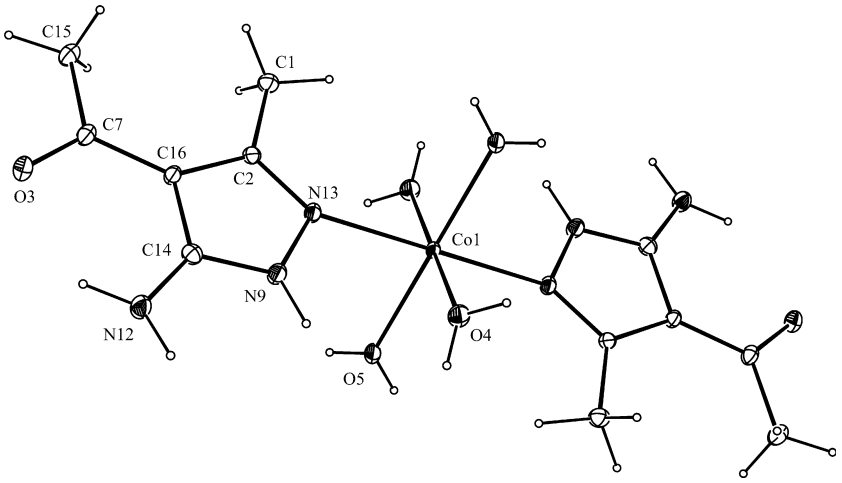

Fig. 1. Molecular diagram and atom numbering scheme of **1**.

Table 2
Selected bond lengths (Å) and angles (°) for **1**

Co1–O4	2.105(1)	O4–Co1–O5	89.55(5)
Co1–O5	2.066(1)	O4–Co1–N13	85.71(4)
Co1–N13	2.159(1)	O4–Co1–O4^{i}	180.00
O3–C7	1.245(2)	O4–Co1–O5^{i}	90.45(5)
C7–C15	1.504(2)	O4–Co1–N13^{i}	94.29(4)
C7–C16	1.438(2)	O5–Co1–N13	87.03(4)
C14–C16	1.420(2)	O4^{i} –Co1–O5	90.45(5)
N12–C14	1.342(2)	O5–Co1–O5^{i}	180.00
N13–C2	1.320(2)	O5–Co1–N13^{i}	92.97(4)
C1–C2	1.495(2)	O4^{i}–Co1–N13	94.29(4)
C2–C16	1.437(2)	O5^{i} –Co1–N13	92.97(4)
O6–N11	1.256(2)	N13–Co1–N13^{i}	180.00
O8–N11	1.256(2)	O4^{i}–Co1–O5^{i}	89.55(5)
O10–N11	1.241(2)	O4^{i}–Co1–N13^{i}	85.71(4)
N9–C14	1.346(2)	O5^{i}–Co1–N13^{i}	87.03(4)
N9–N13	1.394(2)		

i = 1/2 − *x*, 1/2 − *y*, 1 − *z*.

Table 3
Nonbonding contacts relevant for the association of molecules in **1** in the solid state

D–H···A	D...A (Å)	D–H···A (°)
O4–H10···O8^{i}	2.793(2)	167(3)
O5–H13···O8^{ii}	2.878(2)	164(3)
O5–H15···O3^{iii}	2.664(2)	173(3)
O4–H16···O6	2.759(2)	174(3)

i = 1/2 − *x*, 1/2 + y, 3/2 − *z*; ii = 1/2 − *x*, −1/2 + *y*, 3/2 − *z*; iii = −*x*, −*y*, 1 − *z*.

of hydrogen bonding on the structure of the nitrate is considered, it is interesting to note the difference in the N–O distances. One N–O bond (N11–O10 1.241(2) Å) is shorter than the other two (O6–N11 and O8–N11: 1.256(2) Å). This can be attributed to different involvement of the nitrato oxygens in nonbonding contacts. Two oxygen atoms (O6, O8) form longer N–O bonds and participate in strong hydrogen bonds (Table 3) while O10 positioned at a closer distance to N11, shows weaker hydrogen bonding contacts

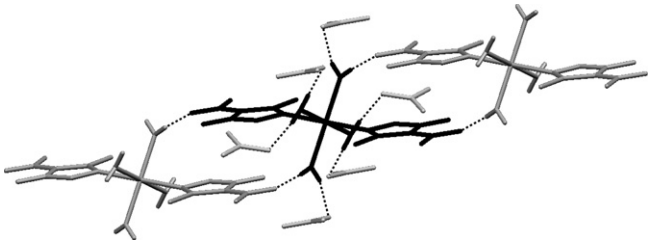

Fig. 2. Part of the crystal structure, showing the contacts relevant for the association of molecules in the crystal structure of **1**. Hydrogen atoms not involved in the nonbonding contacts are excluded for the sake of clarity.

(N12–H5–O10 = 2.25(3)/150(2), N9–H11–O10 = 2.10(3)/148(3) Å).

The *ampf* ligand is bonded to Co(II) in the meridional plane through N10 and acetyl oxygen (O4) and through the imine nitrogen atom (N7), the latter being in *trans* position to one methanol molecule. The distorted octahedral coordination sphere is completed by the axially coordinated nitrate which is in *trans* position to the other methanol molecule. The magnetic moment of the complex ($\mu_{eff} = 5.00\ \mu_B$) is in the accordance with a high-spin Co(II) octahedral geometry. Selected bond lengths are given in Table 4 (see also Table 1 in Supporting information).

The two pyrazole moieties are bound to Co(II) in a different fashion. One pyrazole ring coordinates through the ring nitrogen at a distance of Co–N10 = 2.047(2) Å, while

Table 4
Selected bond lengths (Å) for **2**

	X-ray	Calculated
Co1–O2	2.134(2)	2.004
Co1–O3	2.062(2)	2.111
Co1–O4	2.060(2)	2.145
Co1–O5	2.104(2)	2.342
Co1–N7	2.083(2)	2.156
Co1–N10	2.047(2)	2.096

the other is bound through the acetyl oxygen at a Co–O4 distance of 2.060(2) Å. Different involvement of the acetyl group in bonding is manifested through the differences in the C–O bond lengths (1.242 and 1.225 Å in coordinated and uncoordinated acetyl groups, respectively). However, both acetyl groups show similar twisting relative to the pyrazole ring (2.18° and 3.46°). This feature indicates the relative rigidity of the pyrazole-acetyl fragment, caused by the strong π delocalization. The Co1–O2 distance of the coordinated nitrate is somewhat longer (2.134(2) Å) than the average value for 46 six-coordinated Co(II) nitrate complexes, 2.109(2) Å [32].

Association of the molecules in the crystal lattice is determined by the presence of methanol and nitrate in the axial position of the complex. As can be observed (Fig. 1, Supporting information) O–H···O intermolecular hydrogen bonds (Table 5) are responsible for the self-assembly of the complex molecules into one dimensional chains. The uncoordinated nitrate serves as acceptor of hydrogen bonds donated by the hydrogen atoms of N8 and O3, coordinated in the equatorial plane. The close distance between the ligands in the neighboring molecular chains indicate the existence of π–π interactions. The distance between the ring centroids of the closest pyrazole rings is 3.405(2) Å, with the dihedral angle of 0°. This intermolecular contact leads to formation of chain pairs. However, between the chain pairs there are no significant intermolecular contacts (see Fig. 1 in Supporting information).

The geometrical features of the uncoordinated nitrate show similar pattern as was found in the crystal structure of **1**. Namely, two N–O bonds are longer (1.257, 1.260 Å), than the third one (1.233 Å). This is associated with the different participation in the intermolecular interactions. The two oxygens with longer N–O bonds are involved in strong hydrogen bonds (Table 5), while the oxygen with the shorter N–O bond does not participate in any hydrogen bonds.

Table 5
Nonbonding contacts relevant for the association of molecules in the crystal structure of compound **2**

D–H···A	D...A (Å)	D–H···A (°)
N8–H2···O16	1.980(3)	163.6(3)
O5–H6···O6^{i}	1.936(3)	157.6(3)
O3–H18···O15	1.804(3)	168.6(3)

i = 1 + *x*, *y*, *z*.

3.3. Computed results of **2**: donor–acceptor and hydrogen bonding interactions

Selected computed bond lengths of **2** are compiled in Table 4 (for the other compiled data see Table 1 in Supporting information), facilitating a direct comparison with the experimental ones. The performance of our theoretical level is indicated by the proper agreement (bond distances within 0.02 Å, bond angles within 3°) between the geometrical parameters of the ligand. The deviations are larger for the bond distances and angles associated with the donor–acceptor and hydrogen bonding interactions. It is not surprising, as these looser parameters are more influenced by the inter-complex interactions and packing effects in the crystal. However, the trends in the experimental distances appear also in the computed ones.

Besides, assisting the interpretation of the vibrational spectra, the computations give useful information on the donor–acceptor interactions in the complex molecule. In such systems lacking low-energy π* orbitals, the σ-donation from the ligands is the dominant charge transfer interaction, while the metal-to-ligand back-donation is expected to be negligible. Selected natural atomic charges [27] are given in Table 6. The atomic charge of +1.42 of Co refers to small ligand-to-metal charge transfer in **2** (0.58 e). The energetic contributions of the various charge transfer interactions can be characterized by the second-order perturbation energies [27], the most important

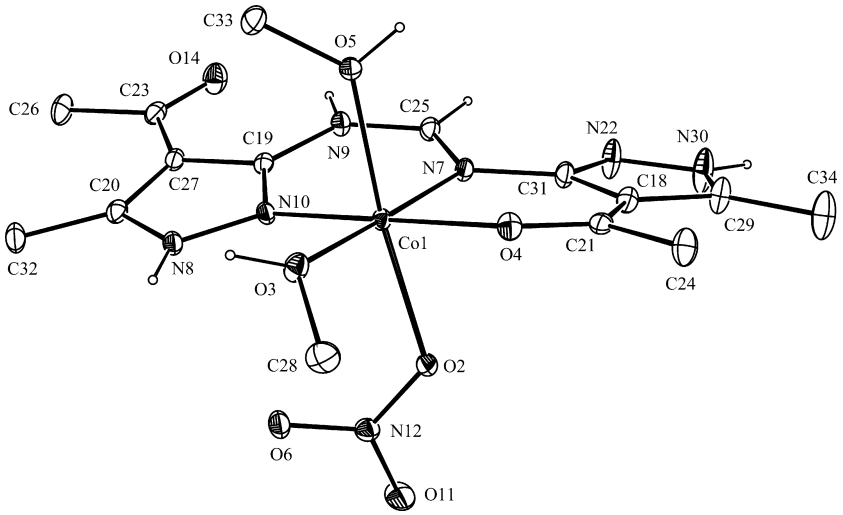

Fig. 3. View of **2** showing the atom numbering scheme. Methyl hydrogen's are excluded for the sake of clarity.

Table 6
Natural atomic charges and charge transfer interactions from the NBO analysis of **2**[a]

Property	Magnitude
qCo	+1.42
qN10	−0.43
qN7	−0.65
qO4	−0.63
qO2	−0.66
qO3	−0.87
qO5	−0.80
$E^{(2)}$ LP(N10) → dCo	61.9
$E^{(2)}$ LP(N7) → dCo	53.9
$E^{(2)}$ LP(O4) → dCo	48.8
$E^{(2)}$ LP(O2) → dCo	83.7
$E^{(2)}$ LP(O3) → dCo	50.5
$E^{(2)}$ LP(O5) → dCo	30.0

[a] Natural charges (q, e) and main second-order perturbation energies ($E^{(2)}$ donor → acceptor, kJ/mol). Computed at the B3LYP/6-31G** level using a relativistic effective core potential for Co. For the numbering of atoms see Fig. 3.

ones compiled in Table 6. They indicate that the six donors (N10, N7, O4, O2, O3 and O5) take part in comparable magnitudes in the total charge transfer, the largest being O2 of the nitrate, while the smallest O5 of MeOH. Note that the MeOH oxygen carries a considerable negative charge as a result of the strongly polarized character of the O–H bond and the inductive effect of the methyl group. The negative charges of the six donor atoms lead to considerable electrostatic attraction between Co(II) and the ligands, contributing, beside the donor–acceptor interactions, to the stability of the complex.

3.4. FT-IR spectrum of 2

The FT-IR spectrum of solid **2** is depicted in Fig. 4, whereas the assignment of the absorption bands is given in Table 7. The assignment was performed on the basis of characteristic group frequencies [33] and the present computed unscaled normal modes. The major part of deviations between the computed and experimental frequencies is in agreement with the harmonic approximation used in the frequency computations. Further differences can originate from the single-molecule model used in the computations in contrast to the crystal, where the unit cell contains four complex molecules. Obviously, in this way the computations cannot take into account the inter-complex (mainly hydrogen bonding) interactions. Yet, the sequence of the theoretical frequencies and the computed IR intensities can assist the assignment in a straightforward way.

The assignment of the ligand modes (Table 7) agrees well with available literature on group frequencies [27]. The strongly red-shifted bands of the N–H and O–H stretching vibrations reflect the strong hydrogen bonding interactions recognized among the X-ray diffraction results. The computations also facilitated the identification of several metal–ligand vibrations in the far-IR spectrum. The stretching metal–ligand vibrations (νCo···N and νCo···O) appear between 400 and 250 cm^{-1}. We could assign three bands to these vibrations, one of them being pure (at 332 cm^{-1}), another one strongly mixed including all the metal–ligand stretchings (at 280 cm^{-1}). Three O–Co–O deformation modes could also be identified at 224, 106 and 89 cm^{-1} in the far-IR spectrum. The assigned bands fall into the range reported previously for related complexes [34].

3.5. UV–Vis spectral studies

Due to their low solubility in cold methanol, the solutions of complexes had to be mildly heated for a short time. During dissolution, the initially orange solutions became pink which remained stable for days.

Electronic spectra of **1** and **2** in methanol (recorded in the range of 220–1400 nm) display several absorption bands. Generally, the two highest energy absorptions,

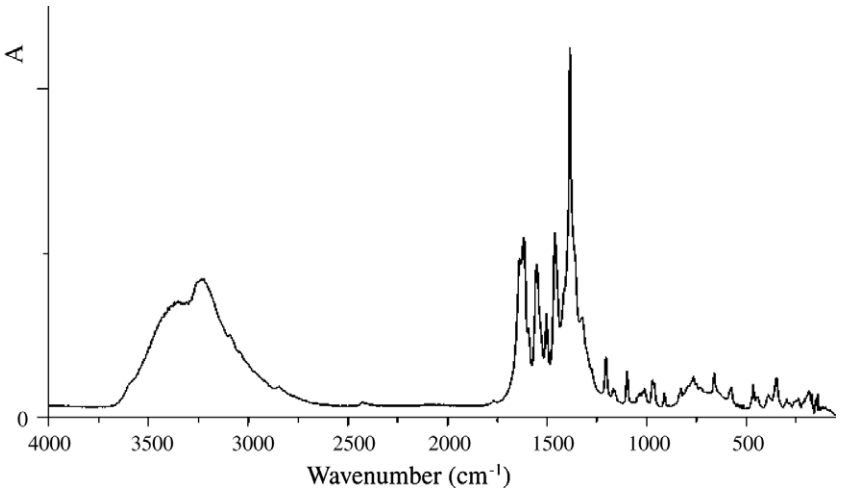

Fig. 4. FT-IR spectrum of **2**.

Table 7
Characteristic bands[a] in the FT-IR spectra of **2**

Experimental	Calculated[b]	Assignment[c]
3376 vs, br	3374 (516)	νN–H, νO–H
3247 vs, br	2977 (2174)	νN–H, νO–H
3086 sh	3170 (3)	νC_{Py}–H
3044 sh	3163 (8)	νC_{Py}–H
2951 sh	3132 (37)	$\nu_{as}CH_3$
2910 sh	3114 (28)	$\nu_{as}CH_3$
2847 w	3054 (178)	$\nu_s CH_3$
1636 s	1715 (675)	νC=O
1615 vs	1672 (723)	νC=N
1593 m	1645 (107)	βN–H
1551 vs	1619 (386)	ν_{as} NO_3^-, βN–H
1530 sh	1614 (386)	βN–H
1501 s	1543 (80)	νPy, $\delta_{as}CH_3$
1460 vs	1495 (592)	νPy, βN–H
1449 sh	1502 (84)	$\delta_{as}CH_3$
1407 sh	1469 (84)	$\delta_{as}CH_3$
1384 vs	1353 (565)	ν_{as} NO_3^-, βOH
1360 sh	1397 (122)	$\delta_s CH_3$
1333 sh	1358 (31)	νPy, νC_{Py}–$C_{C=O}$
1314 s	1343 (76)	ν_{as} NO_3^-, βOH
1275 sh	1310 (71)	νC_{Py}–N, δPy, νC_{Py}–$C_{C=O}$
1205 m	1255 (58)	βN9–H, νC=N
1182 w	1212 (56)	νPy(N–N)
1165 w	1170 (12)	$\delta_{rock}CH_3$ of MeOH
1097 m	1114 (36)	δPy, $\delta_{rock}CH_3$
1044 sh	1075 (74)	ν_s NO_3^-, $\delta_{rock}CH_3$ of Py
1034 w	1059 (74)	νC–O of MeOH, $\delta_{rock}CH_3$ of Py
1022 w	1038 (179)	νC–O of MeOH, $\delta_{rock}CH_3$ of Py
1010 w	1007 (14)	γC_{Py}–H
969 sh	978 (50)	$\delta_{rock}CH_3$ of Py
963 m	990 (202)	γN8–H
910 w	923 (42)	βPy, βN7–C25–N9
826 w	850 (64)	γN9–H
750 br	595 (150)	τOH
797 w	793 (22)	βPy, βC25–N7–C31
766 w	776 (17)	βC19–N9–C25, βPy
737 w	739 (10)	β NO_3^-
659 m	659 (43)	νC–C, βC=O, $\delta_{rock}CH_3$ of Py
582 m	588 (61)	τO5H, βC_{Py}–CH_3
574 m	579 (16)	βC–CH_3, βC–$C_{C=O}$, βC_{Py}–N
527 w	533 (8)	βC–CH_3, βC–$C_{C=O}$, βC_{Py}–N
458 sh	463 (7)	βC=O, βC_{Py}–N, βPy, βCNC
450 m	454 (8)	γC_{Py}–N
431 w	435 (8)	βC=O, βC_{Py}–N
426 sh	426 (5)	γC_{Py}–N
373 w	384 (24)	νCo...O3, ν O3H...ONO_2^-
348 sh	366 (15)	βC_{Ac}–CH_3, βCNC
332 m	303 (41)	ν Co...ONO_2^-
327 sh	335 (17)	βC_{Py}–CH_3, γN–CH, γC_{Py}–CH_3
317 sh	325 (15)	βC_{Py}–CH_3
279 w	278 (5)	γC_{Py}–CH_3
261 m, br	262 (36)	νCo...N and νCo...O of all ligands
241 sh	249 (16)	βC_{Py}–CH_3, βC_{Ac}–CH_3
224 w	223 (31)	νN8H...ONO_2^-, βO3–Co–O5
170 m	179 (13)	τCH_3 (all), ν MeOH...ONO_2^-
125 w	148 (7)	τCH_3 of MeOH
106 w	105 (3)	τCH_3 (all), βO2–Co–O5
100 w	98 (9)	τCH_3 (all)
89 w	89 (5)	δ_{rock}O3–Co–O5

[a] In cm^{-1}. The abbreviations for the band intensities vs, s, m, w, sh mean very strong, strong, medium, week, and shoulder respectively.

[b] Computed at the B3LYP/-31G** level using RECP of Hay and Wadt for Co. (multiplicity = 4) The computed IR intensities (km/mol) are given in parentheses.

[c] The abbreviations ν, β, δ, γ, τ, s, as, Py, and Ac mean stretch, in-plane bend, deformation, out-of-plane bend, torsion, symmetric, asymmetric vibrations, pyrazole ring and acetyl group, respectively.

which are different in these complexes, are due to intraligand transitions. These bands for **1** are similar to those of the ligand [λ_{max}/nm (ε/$dm^3\,mol^{-1}\,cm^{-1}$): 240 (6280), 283 (4500)], with a slight shift to higher energies, suggesting relatively strong metal–ligand bonds. Since $\pi(L) \rightarrow Co(II)$ electron transfers are also expected in this range (~280 nm) [35], the slightly changed appearance and λ_{max} position of the band at 282 nm comparing to that of the ligand are in accordance with the weak intensity of the $\pi(L) \rightarrow Co(II)$ transitions. In this frequency range the electronic spectrum of **2** has a different shape and the multiplicity of the bands can be ascribed to a more complex nature of the tridentate ligand.

The pink color of MeOH solutions and the recorded spectra for *d-d* interactions suggest a pseudo-octahedral geometry for both compounds. For this type of high-spin d^7 complexes three basic electron transitions occur at levels $^4T_{2g} \leftarrow {}^4T_{1g}$ (ν_1), $^4A_{2g} \leftarrow {}^4T_{1g}$ (ν_2) and $^4T_{1g}(P) \leftarrow {}^4T_{1g}$ (ν_3) [36]. A typical shape of a d–d band around ν_3 consists of a low energy shoulder and a weak high-energy absorption, probably as a consequence of spin–orbit coupling. This part of the spectra is illustrated in Fig. 2 given in the Supporting information. The first absorption band, located in the near IR range, is very weak and rather broad (about 100 nm), suggesting an apparent degeneracy of this level. The other transitions, due to presumably trigonal distortion, located in the UV range, are probably either masked by strong intraligand transitions or shifted out of the measured range. Hence, as can be seen from the data, appearance of only two separate bands (ν_1 and ν_3), observed in the spectra of **1** and **2** can be explained in the following way. First, $^4A_{2g} \leftarrow {}^4T_{1g}$ (ν_2) is a two-electron transition and therefore weak in intensity. Second, ν_2 and ν_3 are very close, which does not permit a precise determination of the weaker one, ν_2.

3.6. Thermal decomposition

The thermal decomposition of **1** in the whole temperature range has been described in Ref. [15]. Here we give only some comments on the evaporation mechanism of water molecules from **1** compared to the evaporation of MeOH from **2**. Thermal decomposition curves for both **1** and **2** in argon are presented in Fig. 5. Around 500 K their decomposition turns into a highly exothermic process, due to the presence of nitrate.[1] However, the decomposition is not accomplished up to 1000 K.

The evaporation of H_2O from **1** takes place at 380–420 K temperature range with a slightly detectable asymmetry in the corresponding DTG curve. The mass loss of 12.9% is in agreement within experimental error with the theoretical one (13.51%). On the contrary, the departure of

[1] *Caution*: At higher temperatures nitrates may undergo an explosive decomposition, especially in an oxidative atmosphere. For thermal tests, the sample masses should be reduced.

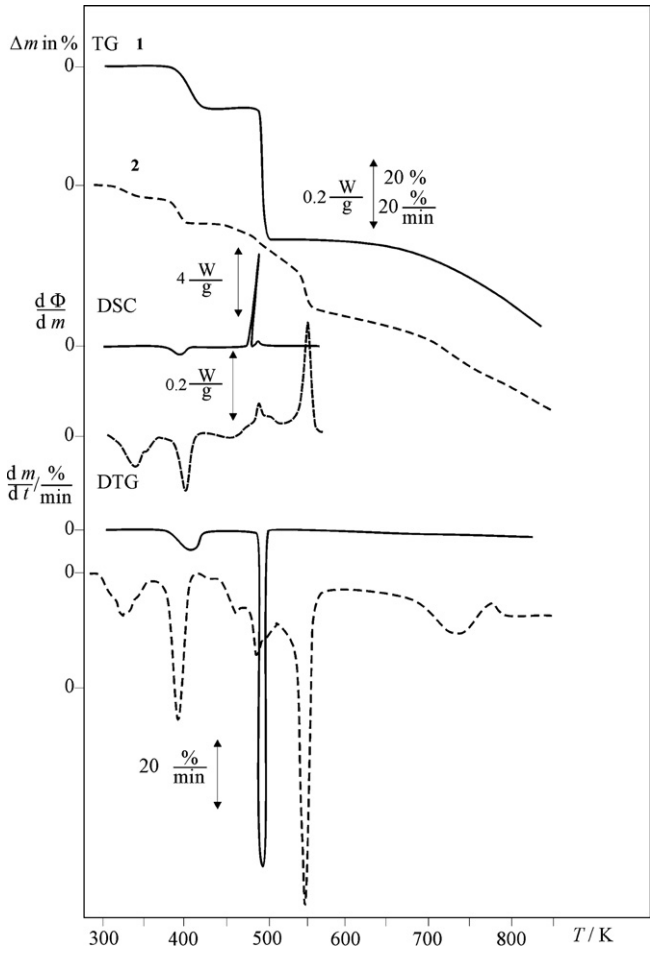

Fig. 5. TA curves of **1** and **2**.

MeOH from **2** takes place in two clearly separated steps: the first, being somewhat slower, begins at 315 K. The second step (another MeOH molecule release) occurs in the temperature range of 380–430 K. The complete mass loss for MeOH (11.2%) is in accordance with the calculated one (11.29%). The evaporation temperature of the first MeOH is close to the boiling point of MeOH (b.p. 337.8 ± 0.3 K) [37]. The evaporation temperature near or above the boiling point of the corresponding solvent supports the fact that the solvent belongs to the inner coordination sphere of the complex [38,39]. The anhydrous Co(*aamp*)$_2$(NO$_3$)$_2$ moiety from **1** is stable in a 50 K temperature range, while the desolvated **2** decomposes onward almost immediately.

We have considered various possibilities for the mechanism of the departure of the solvent molecules in the two complexes. The two-step desolvation mechanism of **2** may origin from the different bonding energies of the two MeOH molecules as indicated by the different Co–O(MeOH) bond lengths (2.104 and 2.062 Å, respectively). This hypothesis is debated by the found one-step desolvation of **1**, where the Co–O(H$_2$O) bond lengths are practically the same as in **2** (2.105 Å for two H$_2$O and 2.066 Å for the other two ones). Yet, only the first MeOH molecule evaporates from 315 K in a range of ca. 70 K, while all four water molecules of **1** depart in a considerably narrow (~40 K) one-step process beginning at 380 K. This may be in accordance with the easier diffusion of the small water molecules through the crystal lattice of **1**, which has a twice larger cell volume than **2** (2110.99 Å^3 and 1099.46 Å^3, respectively. Z: 4, Z': 0 for both compounds). However, it does not explain the significantly higher evaporation temperature of the second MeOH molecule. As the DSC curves (Fig. 5) do not indicate any structural changes during the H$_2$O or MeOH evaporation, most probably other interactions (hydrogen bonds, nonbonding contacts, etc.) play some role in the departure mechanism of the solvent-ligands. As a consequence, only the data of homologue series are comparable.

4. Conclusions

Reaction of Co(NO$_3$)$_2 \cdot$ 6H$_2$O with 4-acetyl-3-amino-5-methylpyrazole (*aamp*) in EtOH and in MeOH, in the presence of CH(OEt)$_3$, gives [Co(*aamp*)$_2$(H$_2$O)$_4$](NO$_3$)$_2$ (**1**), and [Co(*ampf*)(MeOH)$_2$NO$_3$]NO$_3$ (**2**), respectively. The structural properties were studied by X-ray diffraction and in the case of **2**, by quantum chemical computations, too. In **1**, *aamp* acts as a monodentate ligand, binding to the central atom in its usual manner. The coordination sphere of the nearly octahedral complex is completed by the coordination of four water molecules. In an anhydrous solution, in the presence of CH(OEt)$_3$, complex **2** is obtained. Triethyl orthoformate, beside its dehydrating ability, acts as a ligand forming agent: the novel *ampf* ligand is produced in situ, by the fusion of two 4-acetyl-3-amino-5-methylpyrazole molecules through a formamidine bridge formed from their NH$_2$ groups and the methine group of CH(OEt)$_3$. One of the pyrazole derivatives coordinates to Co(II) in an unusual way, through the oxygen atom of the acetyl group. The distorted octahedral geometry of **2** is established by the bonding of the imine nitrogen from the bridging moiety, two MeOH being in *cis* position and a nitrate placed axially. The quantum chemical computations indicate a comparable involvement of the ligand donor atoms in the total charge transfer, and considerable electrostatic attraction between the ligand and the metal in the complex. The IR analysis of **2** and the UV–Vis characterization of both compounds are given. The evaporation of coordinated solvent molecules is discussed.

Acknowledgements

The work was financed by the Ministry for Science of the Republic of Serbia (Grant No. 142028), the Provincial Secretariat for Science and Technological Development of Vojvodina and the Hungarian Scientific Research Foundation (K68332). The authors would like to thank Prof. Ivana Radosavljević Evans (Department of Chemistry, University of Durham, UK) for measuring the crystal data of the compounds.

Appendix A. Supplementary material

CCDC 640905 and 640906 contain the supplementary crystallographic data for **1** and **2**. These data can be obtained free of charge via www.ccdc.cam.ac.uk/data_request/cif, or from the Cambridge Crystallographic Data Centre, 12 Union Road, Cambridge CB2 1EZ, UK; fax: (+44) 1223-336-033; or e-mail: deposit@ccdc.cam.ac.uk. Supplementary data associated with this article can be found, in the online version, at doi:10.1016/j.jorganchem.2007.10.018.

References

[1] A. Hergold-Brundić, B. Kaitner, B. Kamenar, V.M. Leovac, E.Z. Ivegeš, N. Juranić, Inorg. Chim. Acta 188 (1991) 151–158.
[2] V. Yu. Kukushkin, E.A. Aleksandrova, V.M. Leovac, E.Z. Ivegeš, V.K. Belsky, V.K. Konovalov, Polyhedron 11 (1992) 2691–2696.
[3] V.M. Leovac, R. Petković, A. Kovács, G. Pokol, K. Mészáros Szécsényi, J. Therm. Anal. Cal. 89 (2007) 267–275.
[4] N.R. Sperandeo, R. Brun, Chem. Bio. Chem. 4 (2003) 69–72.
[5] D.R. Compton, S. Sheng, K.E. Carlson, N.A. Rebacz, I.Y. Lee, B.S. Katzenellenbogen, J.A. Katzenellenbogen, J. Med. Chem. 47 (2004) 5872–5893.
[6] M. Suzuki, H. Iwasaki, Y. Fujikawa, M. Sakashita, M. Kitahara, R. Sakoda, Bioorg. Med. Chem. Lett. 11 (2001) 1285–1288.
[7] M.E. Fraley, R.S. Rubino, W.F. Hoffman, S.R. Hambaugh, K.L. Arrington, R.W. Hungate, M.T. Bilodeau, A.J. Tebben, R.Z. Rutledge, R.L. Kendall, R.C. McFall, W.R. Huckle, K.E. Coll, K.A. Thomas, Bioorg. Med. Chem. Lett. 12 (2002) 3537–3541.
[8] S. Samanta, B. Debnath, A. Basu, S. Gayen, K. Srikanth, T. Jha, Eur. J. Med. Chem. 41 (2006) 1190–1195.
[9] P. Pevarello, M.G. Brasca, R. Amici, P. Orsini, G. Traquandi, L. Corti, C. Piutti, P. Sansonna, M. Villa, B.S. Pierce, M. Pulici, P. Giordano, K. Martina, E.L. Fritzen, R.A. Nugent, E. Casale, A. Cameron, M. Ciomei, F. Roletto, A. Isacchi, G. Fogliatto, E. Pesenti, W. Pastori, A. Marsiglio, K.L. Leach, P.M. Clare, F. Fiorentini, M. Varasi, A. Vulpetti, M.A. Warpehoski, J. Med. Chem. 47 (2004) 3367–3380.
[10] P. Pevarello, D. Fancelli, A. Vulpetti, R. Amici, M. Villa, V. Pittalà, P. Vianello, A. Cameron, M. Ciomei, C. Mercurio, J.R. Bischoff, F. Roletto, M. Varasi, M.G. Brasca, Bioorg. Med. Chem. Lett. 16 (2006) 1084–1090.
[11] K. Mészáros Szécsényi, V.M. Leovac, V.I. Češljević, A. Kovács, G. Pokol, Gy. Argay, A. Kálmán, G.A. Bogdanović, Ž. K. Jaćimović, A. Spasojević-de Biré, Inorg. Chim. Acta 353 (2003) 253–262.
[12] A. Kovács, D. Nemcsok, G. Pokol, K. Mészáros Szécsényi, V.M. Leovac, Ž. K. Jaćimović, I. Radosavljević Evans, J.A.K. Howard, Z.D. Tomić, G. Giester, New J. Chem. 29 (2005) 833–840.
[13] A. Kovács, K. Mészáros Szécsényi, V.M. Leovac, Z.D. Tomić, G. Pokol, J. Organomet. Chem. 692 (2007) 2582–2592.
[14] V.M. Leovac, E.Z. Ivegeš, V.I. Češljević, A.F. Petrović, D.M. Petrović, D. Poleti, J. Serb. Chem. Soc. 61 (1996) 551–556.
[15] A.F. Petrović, S.R. Lukić, D.M. Petrović, E.Z. Ivegeš, V.M. Leovac, J. Therm. Anal. 47 (1996) 879–886.
[16] Z.D. Tomić, Ž. K. Jaćimović, V.M. Leovac, V.I. Češljević, Acta Crystallogr. C56 (2000) 777–779.
[17] G.A. van Albada, P.J. van Koningsbruggen, I. Mutikainen, U. Turpeinen, J. Reedijk, Eur. J. Inorg. Chem. (1999) 2269–2275.
[18] A. Altomare, G. Cascarano, G. Giacovazzo, A. Guagliardi, M.C. Burla, G. Polidori, M. Camalli, J. Appl. Crystallogr. 27 (1994) 435.
[19] P.W. Betteridge, J.R. Carruthers, R.I. Cooper, K. Prout, D.J. Watkin, J. Appl. Crystallogr. 36 (2003) 1487.
[20] M.N. Burnett, C.K. Johnson, ORTEPIII. Report ORNL-6895. Oak Ridge National Laboratory, Tennessee, USA, 1996.
[21] I.J. Bruno, J.C. Cole, P.R. Edgington, M. Kessler, C.F. Macrae, P. McCabe, J. Pearson, R. Taylor, Acta Crystallogr. B58 (2002) 389–397.
[22] A.D. Becke, J. Chem. Phys. 98 (1993) 5648–5652.
[23] C. Lee, W. Yang, R.G. Parr, Phys. Rev. B37 (1988) 785–789.
[24] P.J. Hay, W.R. Wadt, J. Chem. Phys. 82 (1985) 270–283.
[25] A.W. Ehlers, M. Böhme, S. Dapprich, A. Gobbi, A. Höllwarth, V. Jonas, K.F. Köhler, R. Stegmann, A. Veldkamp, G. Frenking, Chem. Phys. Lett. 208 (1993) 111–114.
[26] M.J. Frisch, G.W. Trucks, H.B. Schlegel, G.E. Scuseria, M.A. Robb, J.R. Cheeseman, J.A. Montgomery Jr., T. Vreven, K.N. Kudin, J.C. Burant, J.M. Millam, S.S. Iyengar, J. Tomasi, V. Barone, B. Mennucci, M. Cossi, G. Scalmani, N. Rega, G.A. Petersson, H. Nakatsuji, M. Hada, M. Ehara, K. Toyota, R. Fukuda, J. Hasegawa, M. Ishida, T. Nakajima, Y. Honda, O. Kitao, H. Nakai, M. Klene, X. Li, J.E. Knox, H.P. Hratchian, J.B. Cross, V. Bakken, C. Adamo, J. Jaramillo, R. Gomperts, R.E. Stratmann, O. Yazyev, A.J. Austin, R. Cammi, C. Pomelli, J.W. Ochterski, P.Y. Ayala, K. Morokuma, G.A. Voth, P. Salvador, J.J. Dannenberg, V.G. Zakrzewski, S. Dapprich, A.D. Daniels, M.C. Strain, O. Farkas, D.K. Malick, A.D. Rabuck, K. Raghavachari, J.B. Foresman, J.V. Ortiz, Q. Cui, A.G. Baboul, S. Clifford, J. Cioslowski, B.B. Stefanov, G. Liu, A. Liashenko, P. Piskorz, I. Komaromi, R.L. Martin, D.J. Fox, T. Keith, M.A. Al-Laham, C.Y. Peng, A. Nanayakkara, M. Challacombe, P.M.W. Gill, B. Johnson, W. Chen, M.W. Wong, C. Gonzalez, J.A. Pople, GAUSSIAN 03, Revision B.05, Gaussian Inc., Wallingford CT, 2004.
[27] A.E. Reed, L.A. Curtiss, F. Weinhold, Chem. Rev. 88 (1988) 899–926.
[28] E.D. Glendening, J.K. Badenhoop, A.E. Reed, J.E. Carpenter, J.A. Bohmann, C.M. Morales, F. Weinhold, NBO 5.0, Theoretical Chemistry Institute, University of Wisconsin, Madison, 2001.
[29] V. Giannouli, I.K. Kostakis, N. Pouli, P. Marakos, O.Ch. Kousidou, G.N. Tzanakakis, N.K. Karamanos, J. Med. Chem. 50 (2007) 1716–1719.
[30] B. Barszcz, T. Glowiak, J. Jezierska, A. Tomkiewicz, Polyhedron 23 (2004) 1309–1316.
[31] G.A. van Albada, S.A. Komaei, H. Kooijman, A.L. Spec, J. Reedijk, Inorg. Chim. Acta 287 (1999) 226–231.
[32] F.J. Barros-García, A. Bernalte-García, F. Luna-Giles, M.A. Maldonado-Rogado, E. Viñuelas-Zahínos, Polyhedron 25 (2006) 52–60.
[33] G. Socrates, Infrared Characteristic Group Frequencies. Tables and Charts, Wiley & Sons, New York, 1994.
[34] K. Nakamoto, Infrared and Raman Spectra of Inorganic and Coordination Compounds. Part B: Applications in Coordination, Organometallic and Bioinorganic Chemistry, Wiley & Sons, New York, 1997, pp. 23–29, 48–50, 57–58.
[35] J.P. Jesson, S. Trofimenko, D.R. Eaton, J. Am. Chem. Soc. 89 (1967) 3148–3158.
[36] A.B.P. Lever, Inorganic Electronic Spectroscopy, Part 1, Sec. Ed., Elsevier, 1967 (Russian translation).
[37] http://webbook.nist.gov/chemistry, 4.02.2007.
[38] H. Icbudak, E. Adiyaman, N. Cetin, A. Bulut, O. Buyukgungor, Trans. Met. Chem. 31 (2006) 666–672.
[39] V.M. Leovac, R. Petković, A. Kovács, G. Pokol, K. Mészáros Szécsényi, J. Therm. Anal. Calorim. 89 (2007) 267–275.